

A Physics-Informed Machine Learning Framework for Safe and Optimal Control of Autonomous Systems

Manan Tayal^{*1}, Aditya Singh^{*1}, Shishir Kolathaya¹, Somil Bansal²

Abstract—As autonomous systems become more ubiquitous in daily life, ensuring high performance with guaranteed safety is crucial. However, safety and performance could be competing objectives, which makes their co-optimization difficult. Learning-based methods, such as Constrained Reinforcement Learning (CRL), achieve strong performance but lack formal safety guarantees due to safety being enforced as soft constraints, limiting their use in safety-critical settings. Conversely, formal methods such as Hamilton-Jacobi (HJ) Reachability Analysis and Control Barrier Functions (CBFs) provide rigorous safety assurances but often neglect performance, resulting in overly conservative controllers. To bridge this gap, we formulate the co-optimization of safety and performance as a state-constrained optimal control problem, where performance objectives are encoded via a cost function and safety requirements are imposed as state constraints. We demonstrate that the resultant value function satisfies a Hamilton-Jacobi-Bellman (HJB) equation, which we approximate efficiently using a novel physics-informed machine learning framework. In addition, we introduce a conformal prediction-based verification strategy to quantify the learning errors, recovering a high-confidence safety value function, along with a probabilistic error bound on performance degradation. Through several case studies, we demonstrate the efficacy of the proposed framework in enabling scalable learning of safe and performant controllers for complex, high-dimensional autonomous systems.

I. INTRODUCTION

Autonomous systems are becoming increasingly prevalent across various domains, from self-driving vehicles and robotic automation to aerospace and industrial applications. Designing control algorithms for these systems involves balancing two fundamental objectives: *performance* and *safety*. Ensuring high performance is essential for achieving efficiency and task objectives under practical constraints, such as fuel limitations or time restrictions. For instance, a warehouse humanoid robot navigating to a destination must optimize its route for efficiency. At the same time, safety remains paramount to prevent catastrophic accidents or system failures. These two objectives, however, often conflict, making it challenging to develop control strategies that achieve both effectively.

A variety of data-driven approaches have been explored to integrate safety considerations into control synthesis. Constrained Reinforcement Learning (CRL) methods [1], [2] employ constrained optimization techniques to co-optimize safety and performance where performance is encoded as a reward function and safety is formulated as a constraint. These methods often incorporate safety constraints into the objective function, leading to only a soft imposition of the safety

constraints. Moreover, such formulations typically minimize cumulative constraint violations rather than enforcing strict safety at all times, which can result in unsafe behaviors.

Another class of methods involve *safety filtering*, which ensures constraint satisfaction by modifying control outputs in real-time. Methods such as Control Barrier Function (CBF)-based quadratic programs (QP) [3] and Hamilton-Jacobi (HJ) Reachability filters [4], [5] act as corrective layers on top of a (potentially unsafe) nominal controller, making minimal interventions to enforce safety constraints. However, because these safety filters operate independently of the underlying performance-driven controller, they often lead to myopic and suboptimal decisions. Alternatively, online optimization-based methods, such as Model Predictive Control (MPC) [6], [7] and Model Predictive Path Integral (MPPI) [8], [9], can naturally integrate safety constraints while optimizing for a performance objective. These methods approximate infinite-horizon optimal control problems (OCPs) with a receding-horizon framework, enabling dynamic re-planning. While effective, solving constrained OCPs online remains computationally expensive, limiting their applicability for high-frequency control applications. The challenge is further exacerbated when dealing with nonlinear dynamics and nonconvex (safety) constraints, limiting the feasibility of these methods for ensuring safety and optimality for real-world systems.

A more rigorous approach to addressing the trade-off between performance and safety is to formulate the problem as a *state-constrained optimal control problem (SC-OCP)*, where safety is explicitly encoded as a hard constraint, while performance is expressed through a reward (or cost) function. While theoretically sound, characterizing the solutions of SC-OCPs is challenging unless certain controllability conditions hold [10]. To address these challenges, [11] proposed an epigraph-based formulation, which characterizes the value function of an SC-OCP by computing its epigraph using dynamic programming, resulting in a Hamilton-Jacobi-Bellman Partial Differential Equation (HJB-PDE). The SC-OCP value function as well as the optimized policy is then recovered from this epigraph. However, dynamic programming suffers from the curse of dimensionality, making it impractical for high-dimensional systems with traditional numerical solvers. Furthermore, the epigraph formulation itself increases the problem's dimensionality, exacerbating computational complexity further.

In this work, we propose a novel algorithmic approach to *co-optimize safety and performance for high-dimensional autonomous systems*. Specifically, we formulate the problem as an SC-OCP and leverage the epigraph formulation in [11]. To efficiently solve this epigraph formulation, we leverage physics-informed machine learning [12], [13] to learn a solution

^{*} Denotes equal contribution.

¹Authors are with the Center for Cyber-Physical Systems, Indian Institute of Science, Bangalore, India (email:{manantayal, adityasingh, shishirk}@iisc.ac.in)

²Author is with the Department of Aeronautics and Astronautics, Stanford University, USA (email:{somil@stanford.edu})

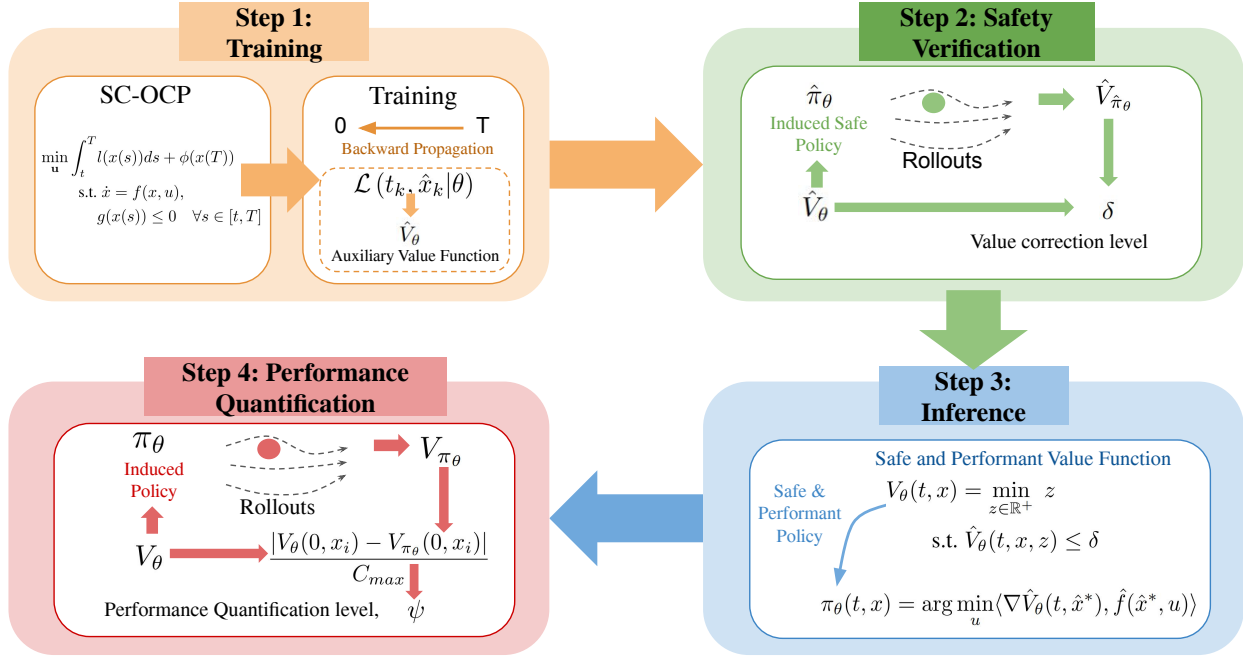


Fig. 1. **Overview of the proposed approach:** The methodology is organized into four steps. The **first step** involves training the auxiliary value function, \hat{V}_θ , using a physics-informed machine learning framework. The **second step** applies a conformal prediction approach for safety verification of the learned \hat{V}_θ . In the **third step**, the final value function V_θ and the optimal safe and performant policy π_θ are inferred. The **fourth step** quantifies the performance of V_θ through a second conformal prediction procedure.

to the resultant HJB-PDE by minimizing PDE residuals. This enables us to efficiently scale epigraph computation for higher-dimensional autonomous systems, leading to safe and performant policies. To summarize, our main contributions are as follows:

- We propose a novel Physics-Informed Machine Learning (PIML) framework to learn policies that co-optimize safety and performance for high-dimensional autonomous systems.
- We introduce a conformal prediction-based safety verification strategy that provides high-confidence probabilistic safety guarantees for the learned policy, reducing the impact of learning errors on safety.
- We propose a performance quantification framework that leverages conformal prediction to provide high-confidence probabilistic error bounds on performance degradation.
- Across three case studies, we showcase the effectiveness of our proposed method in jointly optimizing safety and performance while scaling to complex, high-dimensional systems.

II. PROBLEM SETUP

Consider a nonlinear dynamical system characterized by the state $x \in \mathcal{X} \subseteq \mathbb{R}^n$ and control input $u \in \mathcal{U} \subseteq \mathbb{R}^m$, governed by the dynamics $\dot{x}(t) = f(x(t), u(t))$, where the function $f: \mathbb{R}^n \times \mathbb{R}^m \rightarrow \mathbb{R}^n$ is locally Lipschitz continuous. In this work, we assume that the dynamics model f is known; however, it can also be learned from data if unavailable.

We are given a failure set $\mathcal{F} \subseteq \mathcal{X}$ that represents the set of unsafe states for the system (e.g., obstacles for an autonomous

ground robot). The system's performance is quantified by the cost function $C(t, x, \mathbf{u})$, given by:

$$C(t, x(t), \mathbf{u}) = \int_{s=t}^T l(x(s)) ds + \phi(x(T)), \quad (1)$$

where $l: \mathcal{X} \rightarrow \mathbb{R}_{\geq 0}$ and $\phi: \mathcal{X} \rightarrow \mathbb{R}_{\geq 0}$ are Lipschitz continuous and non-negative functions, representing the running cost over the time horizon $[t, T]$ and the terminal cost at time T , respectively. $\mathbf{u}: [t, T] \rightarrow \mathcal{U}$ is the control signal applied to the system. Using this premise, we define the main objective of this paper:

Objective 1. We aim to synthesize an optimal policy $\pi^*: [t, T] \times \mathcal{X} \rightarrow \mathcal{U}$ that minimizes the cost function C while ensuring that the system remains outside the failure set \mathcal{F} at all times.

A. State-Constrained Optimal Control Problem

To achieve the stated objective, the first step is to encode the safety constraint via a function $g: \mathbb{R}^n \rightarrow \mathbb{R}$ such that, $\mathcal{F} := \{x \in \mathcal{X} \mid g(x) > 0\}$. Using these notations, the objective can be formulated as the following State-Constrained Optimal Control Problem (SC-OCP) to compute the value function V :

$$V(t, x(t)) = \min_{\mathbf{u}} \int_t^T l(x(s)) ds + \phi(x(T)) \quad (2)$$

$$\text{s.t. } \dot{x} = f(x, u),$$

$$g(x(s)) \leq 0 \quad \forall s \in [t, T]$$

This SC-OCP enhances the system's performance by minimizing the cost, while maintaining system safety through the state constraint, $g(x) \leq 0$, ensuring that the system avoids the

failure set, \mathcal{F} . Thus, the policy, π^* , derived from the solution of this SC-OCP co-optimizes safety and performance.

B. Epigraph Reformulation

Directly solving the SC-OCP in (2) presents significant challenges due to the presence of (hard) state constraints. To address this issue, we reformulate the problem in its epigraph form [16], which transforms the constrained optimization into a more tractable two-stage optimization problem. This reformulation allows us to efficiently obtain a solution to the SC-OCP in (2). The resulting formulation is given by:

$$\begin{aligned} V(t, x(t)) = \min_{z \in \mathbb{R}^+} z \\ \text{s.t. } \hat{V}(t, x, z) \leq 0, \end{aligned} \quad (3)$$

where z is a non-negative auxiliary optimization variable, and \hat{V} represents the auxiliary value function. Here, \hat{V} is defined as [11]:

$$\hat{V}(t, x(t), z) = \min_{\mathbf{u}} \max \{ C(t, x(t), \mathbf{u}) - z, \max_{s \in [t, T]} g(x(s)) \}. \quad (4)$$

Note that if $\hat{V}(t, x, z) < 0$, it implies that $g(x(s)) < 0$ for all $s \in [t, T]$. In other words, the system must be outside the failure set at all times; therefore, the system is guaranteed to be safe whenever $\hat{V}(t, x, z) < 0$.

In this reformulated problem, state constraints are effectively eliminated, enabling the use of dynamic programming to characterize the value function, as we explain later in this section. Intuitively, optimal z (z^*) can be thought of as the *minimum permissible cost* the policy can incur without compromising on safety. From Equation 3, it can be inferred that if $z > z^*$, the safety constraint dominates in the max term, resulting in a conservative policy. Conversely, if $z < z^*$, the performance objective takes precedence, leading to a potentially aggressive policy that might compromise safety.

Furthermore, to facilitate solving the epigraph reformulation, z can be treated as a state variable, with its dynamics given by $\dot{z}(t) = -l(x(t))$. This implies that as the trajectory progresses over time, the minimum permissible cost, z , decreases by the step cost $l(x)$ at each time step. This allows us to define an augmented system that evolves according to the following dynamics:

$$\dot{\hat{x}} = \hat{f}(t, \hat{x}, u) := \begin{bmatrix} f(t, x, u) \\ -l(x) \end{bmatrix}, \quad (5)$$

where $\hat{x} := [x, z]^T$ represents the augmented state. With the augmented state representation, it has been shown that the auxiliary value function $\hat{V}(t, x(t), z(t))$ is characterized as the unique continuous viscosity solution of the following Hamilton-Jacobi-Bellman (HJB) partial differential equation (PDE) [11]:

$$\min \left(-\partial_t \hat{V} - \min_{\mathbf{u}} \langle \nabla_{\hat{x}} \hat{V}(t, \hat{x}), \hat{f}(\hat{x}, u) \rangle, \hat{V} - g(x) \right) = 0, \quad (6)$$

$\forall t \in [0, T]$ and $\hat{x} \in \mathcal{X} \times \mathbb{R}$, where $\langle \cdot, \cdot \rangle$ denotes the dot product of vectors. The boundary condition for the PDE is given by:

$$\hat{V}(T, \hat{x}) = \max(\phi(x) - z, g(x)), \quad \hat{x} \in \mathcal{X} \times \mathbb{R}. \quad (7)$$

Note that by a slight abuse of notations, we have replaced the arguments x, z for \hat{V} with the augmented state \hat{x} .

III. METHODOLOGY

To solve the SC-OCP in Equation (2), we aim to compute the optimal value function V , which minimizes the cost while ensuring system safety. In this section, we outline a structured approach: first, we learn the auxiliary value function \hat{V} using a physics-informed machine learning framework. Then, we apply a conformal prediction-based method to verify safety and correct for potential learning errors in \hat{V} . The final value function V is obtained from the safety-corrected \hat{V} using the epigraph formulation in (3). Lastly, we assess the performance of V through a second conformal prediction procedure. Figure 1 gives an overview of the proposed approach.

The following subsections provide a detailed explanation of each step, beginning with the methodology for learning \hat{V} .

A. Training the Auxiliary Value Function (\hat{V})

The auxiliary value function, \hat{V} , satisfies the HJB-PDE in Equation (6), as discussed in Section II-B. Traditionally, numerical methods are used to solve the HJB-PDE over a grid representation of the state space [17], [18], where time and spatial derivatives are approximated numerically. While grid-based methods are accurate for low-dimensional problems, they struggle with the curse of dimensionality – their computational complexity increases exponentially with the number of states – limiting their use in high-dimensional systems. To address this, we adopt a physics-informed machine learning framework inspired by [19], [20], which has proven effective for high-dimensional reachability problems.

The solution of the HJB-PDE inherently evolves backward in time, as the value function at time t is determined by its value at $t + \Delta t$. To facilitate neural network training, we use a curriculum learning strategy, progressively expanding the time sampling interval from the terminal time $[T, T]$ to the full time horizon $[0, T]$. This approach allows the neural network to first accurately learn the value function from the terminal boundary conditions, subsequently propagating the solution backward in time by leveraging the structure of the HJB-PDE.

Specifically, the auxiliary value function is approximated by a neural network, \hat{V}_θ , where θ denotes the trainable parameters of the network. Training samples, $(t_k, x_k, z_k)_{k=1}^N$, are randomly drawn from the state space based on the curriculum training scheme. The proposed learning framework utilizes a loss function that enforces two primary objectives: (i) compliance with the PDE in (6), using the PDE residual error given by:

$$\mathcal{L}_{pde}(t_k, \hat{x}_k | \theta) = \left\| \min \left\{ -\partial_t \hat{V}_\theta(t_k, \hat{x}_k) - H(t_k, \hat{x}_k), \hat{V}_\theta(t_k, \hat{x}_k) - g(x_k) \right\} \right\|, \quad (8)$$

where $H(t, \hat{x}) = \min_{u \in \mathcal{U}} \langle \nabla \hat{V}_\theta(t, \hat{x}), \hat{f}(\hat{x}, u) \rangle$ and (ii) satisfaction of the boundary condition in (7), using boundary condition loss, given by:

$$\mathcal{L}_{bc}(t_k, \hat{x}_k | \theta) = \left\| \max(\phi(x_k) - z_k, g(x_k)) - \hat{V}_\theta(t_k, \hat{x}_k) \right\| \mathbf{1}(t_k = T). \quad (9)$$

These terms are balanced by a trade-off parameter λ , leading to the overall loss function:

$$\mathcal{L}(t_k, \hat{x}_k | \theta) = \mathcal{L}_{pde}(t_k, \hat{x}_k | \theta) + \lambda \mathcal{L}_{bc}(t_k, \hat{x}_k | \theta) \quad (10)$$

Algorithm 1 Safety Verification using Conformal Prediction

Require: \mathcal{S} , N_s , β_s , ϵ_s , $\hat{V}_\theta(0, \hat{x})$, $\hat{V}_{\hat{\pi}_\theta}(0, \hat{x})$, M (number of δ -levels to search for δ),

- 1: $D_0 \leftarrow$ Sample N_s IID states from $\mathcal{S}_{\delta=0}$
- 2: $\delta_0 \leftarrow \min_{\hat{x}_j \in D_0} \{\hat{V}_\theta(0, \hat{x}_j) : \hat{V}_{\hat{\pi}_\theta}(0, \hat{x}_j) \geq 0\}$
- 3: $\epsilon_0 \leftarrow (14)$ (using $\alpha_{\delta=0}$)
- 4: $\Delta \leftarrow$ Ordered list of M uniform samples from $[\delta_0, 0]$
- 5: **for** $i = 0, 1, \dots, M - 1$ **do**
- 6: **while** $\epsilon_i \leq \epsilon_s$ **do**
- 7: $\delta_i \leftarrow \Delta_i$
- 8: Update α_{δ_i} from δ_i
- 9: $\epsilon_i \leftarrow (14)$ (using α_{δ_i})
- 10: **end while**
- 11: **end for**
- 12: **return** $\delta \leftarrow \delta_i$

Minimizing the overall loss function provides a self-supervised learning mechanism to approximate the auxiliary value function.

B. Safety Verification

The learned auxiliary value function, \hat{V}_θ , induces a policy, $\hat{\pi}_\theta$, that minimizes the Hamiltonian term $H(t, \hat{x})$ in the HJB-PDE. The policy is given by:

$$\hat{\pi}_\theta(t, \hat{x}) = \arg \min_{u \in \mathcal{U}} \langle \nabla \hat{V}_\theta(t, \hat{x}), \hat{f}(\hat{x}, u) \rangle. \quad (11)$$

The rollout cost corresponding to this policy is defined as:

$$\hat{V}_{\hat{\pi}_\theta}(t, \hat{x}) = \max\{C(t, x(t), \mathbf{u}) - z, \max_{s \in [t, T]} g(x(s))\} \Big|_{\mathbf{u}=\hat{\pi}_\theta} \quad (12)$$

Ideally, the rollout cost from a given state under $\hat{\pi}_\theta$ should match the value of the auxiliary value function at that state. However, due to learning inaccuracies, discrepancies can arise. This becomes critical when a state, \hat{x}_i , is deemed safe by the auxiliary value function ($\hat{V}_\theta(t, \hat{x}) \leq 0$) but is unsafe under the induced policy ($\hat{V}_{\hat{\pi}_\theta}(t, \hat{x}) > 0$). To address this, we introduce a uniform value function correction margin, δ , which guarantees that the sub- δ level set of the auxiliary value function remains safe under the induced policy. Mathematically, the optimal δ (δ^*) can be expressed as:

$$\delta^* := \min_{\hat{x} \in \mathcal{X}} \{\hat{V}_\theta(0, \hat{x}) : \hat{V}_{\hat{\pi}_\theta}(0, \hat{x}) \geq 0\} \quad (13)$$

Intuitively, δ^* identifies the tightest level of the value function that separates safe states under $\hat{\pi}_\theta$ from unsafe ones. Hence, any initial state within the sub- δ^* level set is guaranteed to be safe under the induced policy, $\hat{\pi}_\theta^*$. However, calculating δ^* exactly requires infinitely many state-space points. To overcome this, we adopt a conformal-prediction-based approach to approximate δ^* using a finite number of samples, providing a probabilistic safety guarantee. The following theorem formalizes our approach:

Theorem III.1 (Safety Verification Using Conformal Prediction). *Let \mathcal{S}_δ be the set of states satisfying $\hat{V}_\theta(0, \hat{x}) \leq \delta$, and let $(0, \hat{x}_i)_{i=1, \dots, N_s}$ be N_s i.i.d. samples from \mathcal{S}_δ . Define α_δ as the safety error rate among these N_s samples for a given δ*

Algorithm 2 Performance Quantification using Conformal Prediction

Require: \mathcal{S}^* , N_p , β_p , $V_\theta(0, x)$, $V_{\pi_\theta}(0, x)$

- 1: $D \leftarrow$ Sample N_p IID states from $\{x : x \in \mathcal{S}^*\}$
- 2: **for** $i = 0, 1, \dots, N_p - 1$ **do**
- 3: $P_i \leftarrow p_i(0, D)$
- 4: **end for**
- 5: $P \leftarrow P$ sorted in decreasing order
- 6: $\alpha_p \leftarrow \frac{1}{N_p+1}$, $\psi_0 \leftarrow P_0$, $\epsilon_0 \leftarrow (18)$
- 7: **for** $i = 0, 1, \dots, N_p - 1$ **do**
- 8: **while** $\epsilon_i \leq \epsilon_p$ **do**
- 9: $\alpha_p \leftarrow \frac{i+1}{N_p+1}$, $\psi_i \leftarrow P_i$, $\epsilon_i \leftarrow (18)$
- 10: **end while**
- 11: **end for**
- 12: **return** $\psi \leftarrow \psi_i$

level. Select a safety violation parameter $\epsilon_s \in (0, 1)$ and a confidence parameter $\beta_s \in (0, 1)$ such that:

$$\sum_{i=0}^{l-1} \binom{N_s}{i} \epsilon_s^i (1 - \epsilon_s)^{N_s-i} \leq \beta_s, \quad (14)$$

where $l = \lfloor (N_s + 1)\alpha_\delta \rfloor$. Then, with the probability of at least $1 - \beta_s$, the following holds:

$$\mathbb{P}_{\hat{x} \in \mathcal{S}_\delta} \left(\hat{V}(0, \hat{x}_i) \leq 0 \right) \geq 1 - \epsilon_s. \quad (15)$$

The proof is available in Appendix A-A. The safety error rate α_δ is defined as the fraction of samples satisfying $\hat{V}_\theta \leq \delta$ and $\hat{V}_{\hat{\pi}_\theta} \geq 0$ out of the total N_s samples.

Algorithm 1 presents the steps to calculate δ using the approach proposed in this theorem.

C. Obtaining Safe and Performant Value Function and Policy from \hat{V}_θ

Using the δ -level estimate from Algorithm (1), we can finally obtain the safe and performant value function, $V_\theta(t, x)$, by solving the following epigraph optimization problem:

$$V_\theta(t, x) = \min_{z \in \mathbb{R}^+} z \quad (16)$$

s.t. $\hat{V}_\theta(t, x, z) \leq \delta$.

Note that $V_\theta(t, x)$ is trivially ∞ for the states where $\hat{V}_\theta(t, x, z) > \delta$, since such states are unsafe and hence do not satisfy the safety constraint.

In practice, we solve this optimization problem by using a binary search approach on z . The resulting optimal state-feedback control policy, $\pi_\theta : \mathcal{X} \times [t, T] \rightarrow \mathcal{U}$, satisfying Objective (1), is given by:

$$\pi_\theta(t, x) = \arg \min_u \langle \nabla \hat{V}_\theta(t, \hat{x}^*), \hat{f}(\hat{x}^*, u) \rangle, \quad (17)$$

where \hat{x}^* is the augmented state associated with the optimal z^* obtained by solving (16), i.e., $\hat{x}^* = [x, z^*]^T$. Intuitively, we can expect π_θ to learn behaviors that best tradeoff the safety and performance of the system.

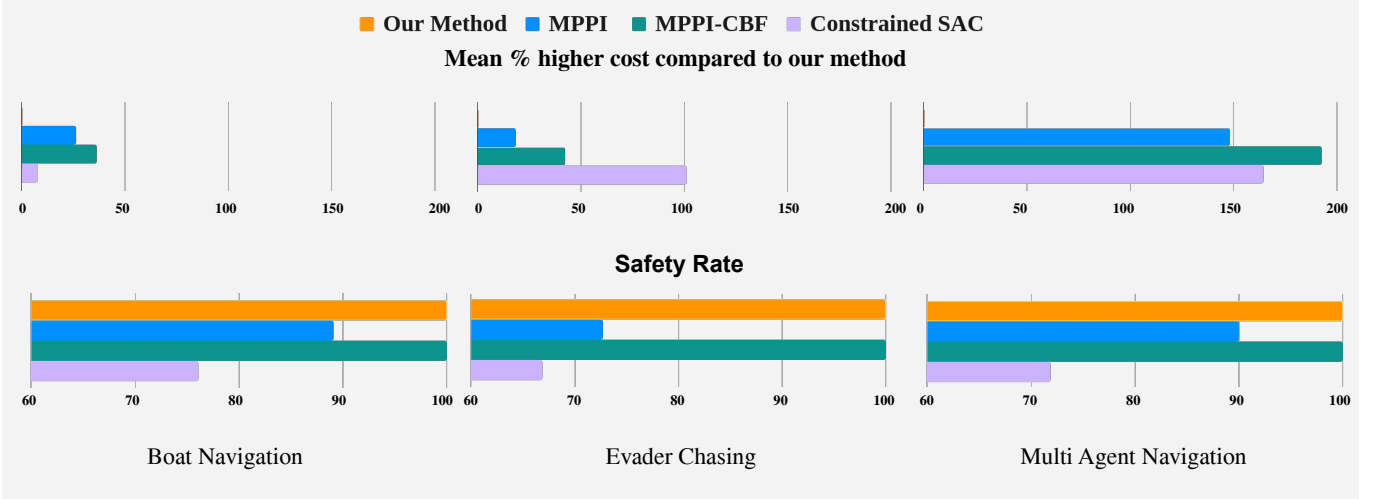


Fig. 2. This figure presents a comparative study between all the methods based on our evaluation metrics. The top plot illustrates the **mean percentage increase in cumulative cost** relative to our method for each baseline, demonstrating that our approach consistently incurs lower costs, with the gap widening as system complexity grows. The bottom plot depicts the **safety rates**, showing that our method maintains a 100% safety rate, while baselines that encourage safety rather than enforcing it (like MPPI and C-SAC) achieve lower rates. MPPI-CBF also attains 100% safety but at the expense of performance. Overall, our method uniquely **balances both safety and performance**, whereas the baselines compromise on at least one aspect.

D. Performance Quantification

In general, the learning inaccuracies in the auxiliary value function \hat{V}_θ , may lead to errors in the value function V_θ . These errors, in turn, can lead to performance degradation under policy π_θ . To quantify this degradation, we propose a conformal prediction-based performance quantification method that provides a probabilistic upper bound on the error between the value function and the value obtained from the induced policy. The following theorem formalizes our approach:

Theorem III.2 (Performance Quantification Using Conformal Prediction). *Suppose \mathcal{S}^* denotes the safe states satisfying $V_\theta(0, x) < \infty$ (or equivalently $\hat{V}_\theta(0, \hat{x}^*) < \delta$) and $(0, x_i)_{i=1, \dots, N_p}$ are N_p i.i.d. samples from \mathcal{S}^* . For a user-specified level α_p , let ψ be the $\frac{\lceil (N_p+1)(1-\alpha_p) \rceil}{N_p}$ th quantile of the scores $(p_i := \frac{|V_\theta(0, x_i) - V_{\pi_\theta}(0, x_i)|}{C_{max}})_{i=1, \dots, N_p}$ on the N_p state samples. Select a violation parameter $\epsilon_p \in (0, 1)$ and a confidence parameter $\beta_p \in (0, 1)$ such that:*

$$\sum_{i=0}^{l-1} \binom{N_p}{i} \epsilon_p^i (1 - \epsilon_p)^{N_p - i} \leq \beta_p \quad (18)$$

where, $l = \lfloor (N_p + 1)\alpha_p \rfloor$. Then, the following holds, with probability $1 - \beta_p$:

$$\mathbb{P}_{x \in \mathcal{S}^*} \left(\frac{|V_\theta(0, x_i) - V_{\pi_\theta}(0, x_i)|}{C_{max}} \leq \psi \right) \geq 1 - \epsilon_p. \quad (19)$$

where C_{max} is a normalizing factor and denotes the maximum possible cost that could be incurred for any $x \in \mathcal{S}^*$.

The proof is available in Appendix A-B. Note that C_{max} can be easily calculated by calculating the upper bound of the cost function $C(t, x(t), \mathbf{u}) \forall x \in \mathcal{S}^*$.

Intuitively, the performance of the resultant policy is the best when the ψ value approaches 0, while the worst performance occurs at $\psi = 1$. Algorithm 2 presents the steps to calculate ψ using the approach proposed in this theorem.

IV. EXPERIMENTS

The objective of this paper is to demonstrate the co-optimization of performance and safety. To achieve this, we evaluate the proposed method and compare them with baselines using two metrics: (1) **Cumulative Cost**: This metric represents the total cost $\int_0^T l(x(s))ds + \phi(x(T))$, accumulated by a policy over the safe trajectories. (2) **Safety Rate**: This metric is defined as the percentage of trajectories that remain safe, i.e., never enter the failure region \mathcal{F} at any point in time.

Baselines: We consider two categories of baselines: the first set of methods aim to enhance the system performance (i.e., minimize the cumulative cost) while encouraging safety, encompassing methods such as Constrained Reinforcement Learning (CRL) and Model Predictive Path Integral (MPPI) [8] algorithms. The second category prioritizes safety, potentially at the cost of performance. This includes safety filtering techniques such as Control Barrier Function (CBF)-based quadratic programs (QP) [3] that modify a nominal, potentially unsafe controller to satisfy the safety constraint. Additionally, we have presented the comparative study of offline and online computation times between the baselines in Appendix C-E.

A. Efficient and Safe Boat Navigation

In our first experiment, we consider a 2D autonomous boat navigation problem, where a boat with coordinates (x_b, y_b) navigates a river with state-dependent drift to reach an island. The boat must avoid two circular boulders (obstacles) of different radii, which corresponds to the safety constraint in the system (see Fig. 3). The cost function penalizes the distance to the goal. The system state, x , evolves according to the dynamics:

$$x = [x_b, y_b], \quad \dot{x} = [u_1 + 2 - 0.5y_b^2, u_2] \quad (20)$$

where $[u_1, u_2]$ are the bounded control inputs in the x_b and y_b directions, constrained by the control space $\mathcal{U} = \{[u_1, u_2] \in \mathbb{R}^2 \mid \|[u_1, u_2]\| \leq 1\}$. The term $2 - 0.5y_b^2$ introduces a state-dependent drift, complicating the control task as the

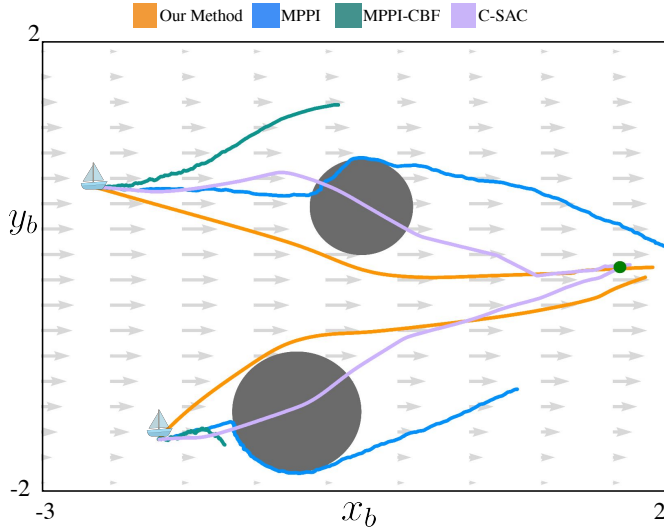


Fig. 3. Trajectories from two distinct initial states are shown, with dark grey circles representing obstacles and the green dot indicating the goal at $[1.5, 0]^T$. Notably, our method is the **only one** that **successfully approaches the goal** while **adhering to safety constraints**.

actions must counteract the drift while ensuring safety, which is challenging under bounded control inputs. The rest of the details about the experiment setup can be found in the Appendix B-A.

Safety Guarantees and Performance Quantification: We use $N_s = 300K$ and $N_p = 300K$ samples for thorough verification, ensuring dense state space sampling. For this experiment, we set $\epsilon_s = 0.001$ and $\beta_s = 10^{-10}$, resulting in a δ -level of 0. This implies that, with $1 - 10^{-10}$ confidence, any state with $\hat{V}_\theta(t, x, z) \leq 0$, is safe with at least 99.9% probability. For performance quantification, we set $\epsilon_p = 0.01$ and $\beta_p = 10^{-10}$, leading to a ψ -level of 0.136. This ensures, with $1 - 10^{-10}$ confidence, that any state in \mathcal{S}^* has a normalized error between the predicted value and the policy value of less than 0.136 with 99% probability. Low δ and ψ values with high confidence indicate that the learned policy closely approximates the optimal policy and successfully co-optimizes safety and performance.

Baselines: This being a 2-dimensional system, we compare our method with the ground truth value function computed by solving the HJB-PDE numerically using the Level Set Toolbox [17] (results in Appendix B-A1). Additional baselines include: (1) MPPI, a sample-based path-planning algorithm with safety as soft constraints, (2) MPPI-NCBF, where safety is enforced using a Neural CBF-based QP with MPPI as the nominal controller [21], [22], and (3) C-SAC, a Lagrangian-based CRL approach using Soft Actor-Critic [23], incorporating safety as soft constraints.

Comparative Analysis: Figure 3 shows that our method effectively reaches the goal while avoiding obstacles, even when starting close to them. In contrast, MPPI and C-SAC-based policies fail to maintain safety, while MPPI-NCBF ensures safety but performs poorly (leading to very slow trajectories). Figure 2 highlights that our method outperforms all others. C-SAC achieves reasonable performance with a 7.5% higher mean cost compared to ours but has the lowest safety rate

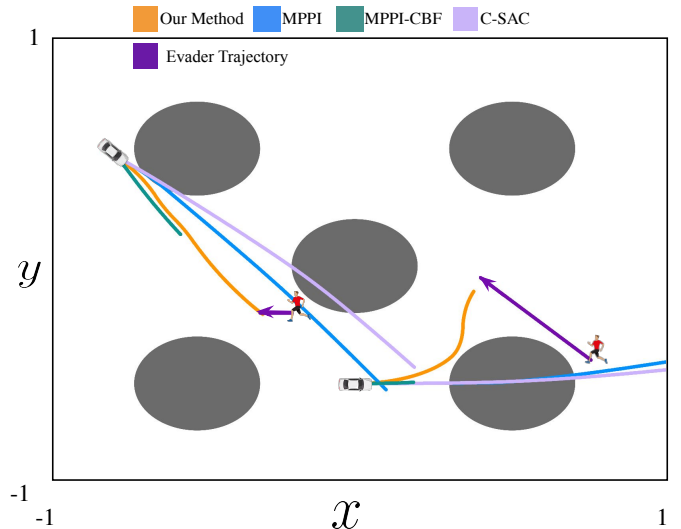


Fig. 4. Trajectories from two distinct initial states are depicted, with dark grey circles representing obstacles and purple trajectories indicating the evader's path, with arrows showing its direction of motion. Our method successfully **tracks the evader** while **avoiding collisions**, whereas all other methods either fail to maintain safety, struggle to track the evader or both

of 76%. MPPI, with a more competitive safety rate of 89%, performs poorly with a 32.67% higher mean cost. MPPI-NCBF achieves 100% safety but performs significantly worse, with a 50.72% higher mean cost. Additionally, CBF-based controllers sometimes violate control bounds, limiting their applicability. This demonstrates that our method balances safety and performance, unlike others that compromise on one aspect. Moreover, the 100% safety rate of our method aligns closely with at least 99.9% safety level that we expect using our proposed verification strategy, providing empirical validation of the safety assurances.

B. Pursuer Vehicle tracking a moving Evader

In our second experiment, we consider an acceleration-driven pursuer vehicle, tracking a moving evader while avoiding five circular obstacles (see Fig. 4). This experiment involves an 8-dimensional system, with the state x defined as $x = [x_p, y_p, v, \Theta, x_e, y_e, v_{x_e}, v_{y_e}]^T$, where x_p, y_p, v, Θ represent the coordinates, linear velocity, and orientation of the pursuer vehicle, respectively, and $x_e, y_e, v_{x_e}, v_{y_e}$ represent the coordinates and linear velocities of the evader vehicle. The pursuer vehicle is controlled by linear acceleration (u_1) and angular velocity (u_2). The control space is $\mathcal{U} = \{[u_1, u_2] \in [-2, 2]^2\}$. The complexity of this system stems from the dynamic nature of the goal, along with the challenge of ensuring safety in a cluttered environment, which in itself is a difficult safety problem. More details about the experiment setup are in Appendix B-B.

Safety Guarantees and Performance Quantification: Similar to the previous experiment, we set $N_s = N_p = 300k$. We choose $\epsilon_s = 0.01$ and $\beta_s = 10^{-10}$, yielding a δ -level of -0.04 and a safety level of 99% on the auxiliary value function. For performance, we set $\epsilon_p = 0.01$ and $\beta_p = 10^{-10}$, leading to a ψ -level of 0.137. These values indicate the learned policy maintains high safety with low-performance degradation in this cluttered environment.

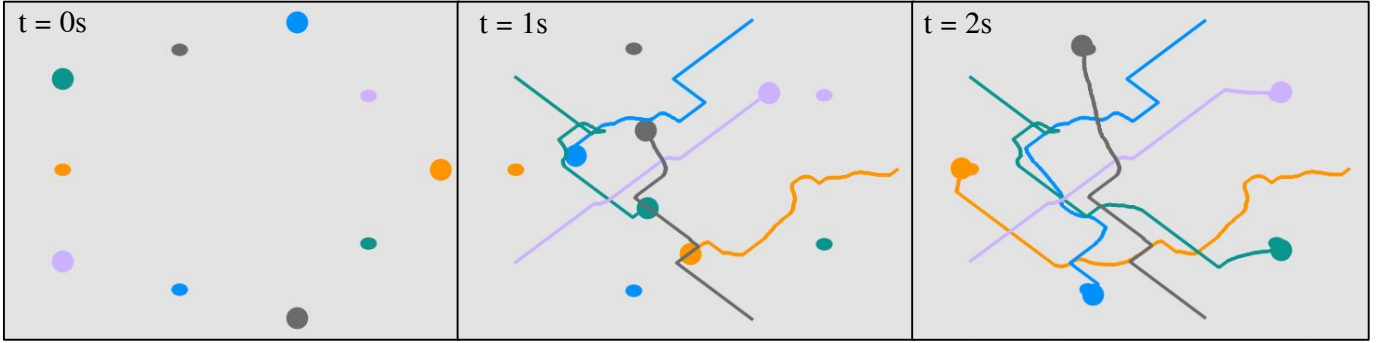


Fig. 5. Snapshots of multi-agent navigation trajectories at different times using the proposed method. Agents are represented as circles with radius R , indicating the minimum safe distance they must maintain from each other. Smaller dots mark their respective goals. The trajectories show that agents proactively **maintain long-horizon safety** by adjusting their paths to avoid close encounters, rather than enforcing safety reactively, which could lead to suboptimal behaviors. Finally, the agents **reach their respective goals within the specified time horizon**.

Baselines: Similar to the previous experiment, we use MPPI and C-SAC with soft safety constraints as our baselines. For safety filtering, we apply a collision cone CBF (C3BF) [24]-based QP due to its effectiveness in handling acceleration-driven systems.

Comparative Analysis: Figure 4 shows that our method effectively tracks the moving evader while avoiding obstacles, even when starting close to them. In contrast, other methods have limitations: MPPI and C-SAC attempt to follow the evader but fail to maintain their pace, violating safety constraints, while MPPI-C3BF sacrifices performance to maintain safety. Figure 2 highlights our method’s superior performance in balancing safety and performance. MPPI achieves the best performance among the baselines but with an 18% higher mean cost and only a 72% safety rate. MPPI-NCBF ensures 100% safety but has a 42% higher mean cost. C-SAC underperforms both in safety (66% safety rate) and performance (101% higher mean cost). This suggests that C-SAC struggles with co-optimizing safety and performance optimization in high-dimensional, complex systems. Additionally, the safety guarantees hold true in the test samples, confirming the reliability of our proposed safety verification framework in safety-critical, cluttered environments.

Receding Horizon Control: An interesting application of the synthesized policy is its deployment in a receding horizon fashion over a time horizon longer than that used for training the value function, as illustrated in Fig. 6. The results indicate that the learned policy successfully maintains safety while effectively tracking the evader over a 6-second horizon, despite being trained over a horizon of 1 second. This suggests that the proposed approach can be extended to effectively co-optimize safety and performance for long-horizon tasks by solving the SC-OCF over a shorter time horizon. Consequently, this framework offers a practical solution for real-world autonomous systems that require long-horizon safety and performance guarantees.

C. Multi-Agent Navigation

In our third experiment, we consider a multi-agent setting where each of the 5 agents, represented by $x_i = [x_{a_i}, y_{a_i}, x_{g_i}, y_{g_i}]$, tries to reach its goal while avoiding collisions with others. (x_{a_i}, y_{a_i}) denote the position of the i th agent, while (x_{g_i}, y_{g_i}) represent the goal locations for that agent. The system is 20-dimensional, with each agent controlled

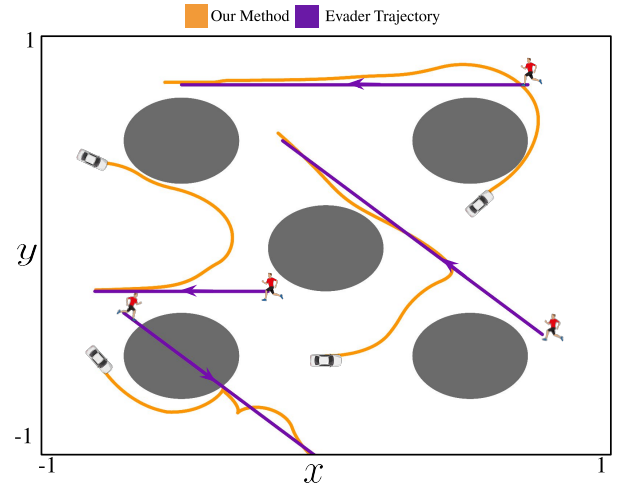


Fig. 6. Trajectories of the **receding horizon policy** for the pursuer tracking an evader over a 6-second horizon, while the value function is trained over a 1-second horizon. The results demonstrate that the pursuer **successfully tracks** the evader while ensuring safety, even when initialized near the obstacle. This highlights the effectiveness of the proposed approach in **jointly optimizing safety and performance for long-horizon tasks**.

by its x and y velocities. The control space for each agent is $\mathcal{U}_i = \{[v_{x_i}, v_{y_i}] \mid \|[v_{x_i}, v_{y_i}]\| \leq 1\}$. The complexity of this system stems from the interactions and potential conflicts between agents as they attempt to reach their goals while avoiding collisions. The rest of the details about the experiment setup can be found in Appendix B-C.

Safety Guarantees and Performance Quantification: We set $N_s = N_p = 300k$, $\epsilon_s = 0.001$, and $\beta_s = 10^{-10}$, resulting in a δ -level of -0.09 with safety assurance of 99.9% for the auxiliary value function. For performance quantification, we set $\epsilon_p = 0.01$ and $\beta_p = 10^{-10}$, leading to a ψ -level of 0.068. It is evident that the δ and ψ values remain very low with high confidence, highlighting the effectiveness of our method in co-optimizing safety and performance for high-dimensional, multi-agent systems.

Baselines: Similar to previous experiments, we have used MPPI, C-SAC, and MPPI-NCBF as our baselines for this experiment too.

Comparative Analysis: Figure 5 shows that our method ensures long-horizon safety while enabling all agents to reach their goals without collisions. In contrast, the baseline methods either exhibit overly conservative behavior or fail to maintain safety,

leading to collisions, as detailed in Appendix C-F. Figure 2 demonstrates the superior performance of our approach, with MPPI, MPPI-NCBF, and C-SAC showing mean percentage cost increases of 148%, 192%, and 164%, respectively. Although MPPI and MPPI-NCBF achieve competitive safety rates of 90% and 100%, their significant performance degradation highlights their inability to balance safety and performance in complex systems. MPPI's subpar performance stems from its reliance on locally optimal solutions in a finite data regime, leading to several deadlocks along the way and overall suboptimal trajectories over a long horizon. Furthermore, C-SAC struggles with both safety and performance, further demonstrating its limitations in handling increasing system complexity and dimensionality. These results confirm our method's ability to co-optimize safety and performance in high-dimensional systems, demonstrating its scalability. Additionally, the safety guarantees hold in the test samples, validating the scalability of our safety verification framework for multi-agent systems.

V. CONCLUSION AND FUTURE WORK

In this work, we introduced a physics-informed machine learning framework for co-optimizing safety and performance in autonomous systems. By formulating the problem as a state-constrained optimal control problem (SC-OCP) and leveraging an epigraph-based approach, we enabled scalable computation of safety-aware policies. Our method integrates conformal prediction-based safety verification to ensure high-confidence safety guarantees while maintaining optimal performance. Through multiple case studies, we demonstrated the effectiveness and scalability of our approach in high-dimensional systems. In future, we will explore methods for rapid adaptation of the learned policies in light of new information about the system dynamics, environments, or safety constraints. We will also apply our method to other high-dimensional autonomous systems and systems with unknown dynamics.

REFERENCES

- [1] E. Altman, *Constrained Markov Decision Processes*, ser. Stochastic Modeling Series. Taylor & Francis, 1999. [Online]. Available: <https://books.google.co.in/books?id=3X9S1NM2iOgC>
- [2] J. Achiam, D. Held, A. Tamar, and P. Abbeel, "Constrained policy optimization," in *International conference on machine learning*. PMLR, 2017, pp. 22–31.
- [3] A. D. Ames, X. Xu, J. W. Grizzle, and P. Tabuada, "Control barrier function based quadratic programs for safety critical systems," *IEEE Transactions on Automatic Control*, vol. 62, no. 8, pp. 3861–3876, 2017.
- [4] J. Borquez, K. Chakraborty, H. Wang, and S. Bansal, "On safety and liveness filtering using hamilton-jacobi reachability analysis," *IEEE Transactions on Robotics*, vol. 40, pp. 4235–4251, 2024.
- [5] K. P. Wabersich, A. J. Taylor, J. J. Choi, K. Sreenath, C. J. Tomlin, A. D. Ames, and M. N. Zeilinger, "Data-driven safety filters: Hamilton-jacobi reachability, control barrier functions, and predictive methods for uncertain systems," *IEEE Control Systems Magazine*, vol. 43, no. 5, pp. 137–177, 2023.
- [6] C. E. García, D. M. Prett, and M. Morari, "Model predictive control: Theory and practice—a survey," *Automatica*, vol. 25, no. 3, pp. 335–348, 1989. [Online]. Available: <https://www.sciencedirect.com/science/article/pii/0005109889900022>
- [7] L. Grüne, J. Pannek, L. Grüne, and J. Pannek, *Nonlinear model predictive control*. Springer, 2017.
- [8] G. Williams, P. Drews, B. Goldfain, J. M. Rehg, and E. A. Theodorou, "Information-theoretic model predictive control: Theory and applications to autonomous driving," *IEEE Transactions on Robotics*, vol. 34, no. 6, pp. 1603–1622, 2018.
- [9] L. Streichenberg, E. Trevisan, J. J. Chung, R. Siegart, and J. Alonso-Mora, "Multi-agent path integral control for interaction-aware motion planning in urban canals," in *2023 IEEE International Conference on Robotics and Automation (ICRA)*, 2023, pp. 1379–1385.
- [10] H. M. Soner, "Optimal control with state-space constraint i," *SIAM Journal on Control and Optimization*, vol. 24, no. 3, pp. 552–561, 1986. [Online]. Available: <https://doi.org/10.1137/0324032>
- [11] A. Altarovici, O. Bokanowski, and H. Zidani, "A general hamilton-jacobi framework for non-linear state-constrained control problems," *ESAIM: Control, Optimisation and Calculus of Variations*, vol. 19, no. 2, pp. 337–357, 2013.
- [12] M. Raissi, P. Perdikaris, and G. Karniadakis, "Physics-informed neural networks: A deep learning framework for solving forward and inverse problems involving nonlinear partial differential equations," *Journal of Computational Physics*, vol. 378, pp. 686–707, 2019. [Online]. Available: <https://www.sciencedirect.com/science/article/pii/S0021999118307125>
- [13] Z. Li, H. Zheng, N. B. Kovachki, D. Jin, H. Chen, B. Liu, A. Stuart, K. Azizzadenesheli, and A. Anandkumar, "Physics-informed neural operator for learning partial differential equations," 2022. [Online]. Available: <https://openreview.net/forum?id=dYnHcmQKMe>
- [14] O. So and C. Fan, "Solving stabilize-avoid optimal control via epigraph form and deep reinforcement learning," in *Robotics: Science and Systems*, 2023.
- [15] M. Tayal, A. Singh, P. Jagtap, and S. Kolathaya, "Semi-supervised safe visuomotor policy synthesis using barrier certificates," *arXiv preprint arXiv:2409.12616*, 2024.
- [16] S. Boyd and L. Vandenberghe, *Convex optimization*. Cambridge university press, 2004.
- [17] I. Mitchell, "A toolbox of level set methods," <http://www.cs.ubc.ca/mitchell/ToolboxLS/toolboxLS.pdf>, 2004.
- [18] E. Schmerling, "hj_reachability: Hamilton-Jacobi reachability analysis in JAX," https://github.com/StanfordASL/hj_reachability, 2021.
- [19] S. Bansal and C. J. Tomlin, "Deepreach: A deep learning approach to high-dimensional reachability," in *2021 IEEE International Conference on Robotics and Automation (ICRA)*, 2021, pp. 1817–1824.
- [20] A. Singh, Z. Feng, and S. Bansal, "Exact imposition of safety boundary conditions in neural reachable tubes," 2024. [Online]. Available: <https://arxiv.org/abs/2404.00814>
- [21] C. Dawson, Z. Qin, S. Gao, and C. Fan, "Safe nonlinear control using robust neural lyapunov-barrier functions," in *Conference on Robot Learning*. PMLR, 2022, pp. 1724–1735.
- [22] M. Tayal, H. Zhang, P. Jagtap, A. Clark, and S. Kolathaya, "Learning a formally verified control barrier function in stochastic environment," in *Conference on Decision and Control (CDC)*. IEEE, 2024.
- [23] T. Haarnoja, A. Zhou, P. Abbeel, and S. Levine, "Soft actor-critic: Off-policy maximum entropy deep reinforcement learning with a stochastic actor," in *Proceedings of the 35th International Conference on Machine Learning*, ser. Proceedings of Machine Learning Research, J. Dy and A. Krause, Eds., vol. 80. PMLR, 10–15 Jul 2018, pp. 1861–1870. [Online]. Available: <https://proceedings.mlr.press/v80/haarnoja18b.html>
- [24] B. G. Goswami, M. Tayal, K. Rajgopal, P. Jagtap, and S. Kolathaya, "Collision cone control barrier functions: Experimental validation on uavs for kinematic obstacle avoidance," in *2024 American Control Conference (ACC)*, 2024, pp. 325–331.
- [25] A. N. Angelopoulos and S. Bates, "A gentle introduction to conformal prediction and distribution-free uncertainty quantification," 2022. [Online]. Available: <https://arxiv.org/abs/2107.07511>
- [26] A. Lin and S. Bansal, "Verification of neural reachable tubes via scenario optimization and conformal prediction," in *Proceedings of the 6th Annual Learning for Dynamics & Control Conference*, ser. Proceedings of Machine Learning Research, A. Abate, M. Cannon, K. Margellos, and A. Papachristodoulou, Eds., vol. 242. PMLR, 15–17 Jul 2024, pp. 719–731. [Online]. Available: <https://proceedings.mlr.press/v242/lin24a.html>
- [27] V. Vovk, "Conditional validity of inductive conformal predictors," 2012. [Online]. Available: <https://arxiv.org/abs/1209.2673>
- [28] F. W. J. Olver, A. B. O. Daalhuis, D. W. Lozier, B. I. Schneider, R. F. Boisvert, C. W. Clark, B. R. Miller, B. V. Saunders, H. S. Cohl, and e. M. A. McClain, *NIST Digital Library of Mathematical Functions*, 2023, release 1.1.11 of 2023-09-15. [Online]. Available: <https://dlmf.nist.gov/>
- [29] H. Wang, A. Dhande, and S. Bansal, "Cooptimizing safety and performance with a control-constrained formulation," *IEEE Control Systems Letters*, vol. 8, pp. 2739–2744, 2024.

APPENDIX A
PROOFS

A. Proof of Theorem (III.1)

Before we proceed with the proof of the Theorem (III.1), let us look at the following lemma which describes split conformal prediction:

Lemma 1 (Split Conformal Prediction [25]). Consider a set of independent and identically distributed (i.i.d.) calibration data, denoted as $\{(X_i, Y_i)\}_{i=1}^n$, along with a new test point $(X_{\text{test}}, Y_{\text{test}})$ sampled independently from the same distribution. Define a score function $s(x, y) \in \mathbb{R}$, where higher scores indicate poorer alignment between x and y . Compute the calibration scores $s_1 = s(X_1, Y_1), \dots, s_n = s(X_n, Y_n)$. For a user-defined confidence level $1 - \alpha$, let \hat{q} represent the $\lceil (n+1)(1-\alpha) \rceil / n$ quantile of these scores. Construct the prediction set for the test input X_{test} as:

$$\mathcal{C}(X_{\text{test}}) = \{y : s(X_{\text{test}}, y) \leq \hat{q}\}.$$

Assuming exchangeability, the prediction set $\mathcal{C}(X_{\text{test}})$ guarantees the marginal coverage property:

$$\mathbb{P}(Y_{\text{test}} \in \mathcal{C}(X_{\text{test}})) \geq 1 - \alpha.$$

Proof. Following the Lemma 1, we employ a conformal scoring function for safety verification [26], defined as:

$$s(X) = \hat{V}_{\hat{\pi}_\theta}(0, \hat{x}), \forall \hat{x} \in \mathcal{S}_\delta,$$

where \mathcal{S}_δ denotes the set of states satisfying $\hat{V}_\theta(0, \hat{x}) \leq \delta$ and the score function measures the alignment between the induced safe policy and the auxiliary value function.

Next, we sample N_s states from the safe set \mathcal{S}_δ and compute conformal scores for all sampled states. For a user-defined error rate $\alpha \in [0, 1]$, let \hat{q} denote the $\frac{(N_s+1)\alpha}{N_s}$ th quantile of the conformal scores. According to [27], the following property holds:

$$\mathbb{P}_{\hat{x} \in \mathcal{S}_\delta} \left(\hat{V}_{\hat{\pi}_\theta}(0, \hat{x}_i) \leq \hat{q} \right) \sim \text{Beta}(N_s - l + 1, l), \quad (21)$$

where $l = \lfloor (N_s + 1)\alpha \rfloor$.

Define E_s as:

$$E_s := \mathbb{P}_{\hat{x} \in \mathcal{S}_\delta} \left(\hat{V}_{\hat{\pi}_\theta}(0, \hat{x}_i) \leq \hat{q} \right).$$

Here, E_s is a Beta-distributed random variable. Using properties of cumulative distribution functions (CDF), we assert that $E_s \geq 1 - \epsilon_s$ with confidence $1 - \beta_s$ if the following condition is satisfied:

$$I_{1-\epsilon_s}(N - l + 1, l) \leq \beta_s, \quad (22)$$

where $I_x(a, b)$ is the regularized incomplete Beta function and also serves as the CDF of the Beta distribution. It is defined as:

$$I_x(a, b) = \frac{1}{B(a, b)} \int_0^x t^{a-1} (1-t)^{b-1} dt,$$

where $B(a, b)$ is the Beta function. From [28](8.17.5), it can be shown that $I_x(n-k, k+1) = \sum_{i=1}^k \binom{n}{i} x^i (1-x)^{n-i}$.

Then (22) can be rewritten as:

$$\sum_{i=1}^{l-1} \binom{N_s}{i} \epsilon_s^i (1-\epsilon)^{N_s-i} \leq \beta_s, \quad (23)$$

Thus, if Equation (23) holds, we can say with probability $1 - \beta_s$ that:

$$\mathbb{P}_{\hat{x} \in \mathcal{S}_\delta} \left(\hat{V}_{\hat{\pi}_\theta}(0, \hat{x}_i) \leq \hat{q} \right) \geq 1 - \epsilon_s. \quad (24)$$

Now, let k denote the cardinality of the set $A = \{x \in \mathcal{S}_\delta \mid \hat{V}_\theta(0, \hat{x}) \leq \delta, \hat{V}_{\hat{\pi}_\theta}(0, \hat{x}) \geq 0\}$. Thus, the safety error rate is given by $\alpha_\delta = \frac{k+1}{N_s+1}$. Let \hat{q} represent the $\frac{(N_s+1)\alpha_\delta}{N_s}$ th quantile of the conformal scores. Since k denotes the number of samples for which the conformal score is positive, the $\frac{(N_s+1)\alpha_\delta}{N_s}$ th quantile of scores corresponds to the maximum *negative score* amongst the sampled states. This implies that $\hat{q} \leq 0$. From this and Equation (24), we can conclude with probability $1 - \beta_s$ that:

$$\mathbb{P}_{\hat{x} \in \mathcal{S}_\delta} \left(\hat{V}_{\hat{\pi}_\theta}(0, \hat{x}_i) \leq 0 \right) \geq 1 - \epsilon_s.$$

From Equation (4), it can be inferred that $\forall (t, \hat{x}), \hat{V}(t, \hat{x}) \leq \hat{V}_{\hat{\pi}_\theta}(0, \hat{x})$. Hence, with probability $1 - \beta_s$, the following holds:

$$\mathbb{P}_{\hat{x} \in \mathcal{S}_\delta} \left(\hat{V}(0, \hat{x}_i) \leq 0 \right) \geq 1 - \epsilon_s.$$

□

B. Proof of Theorem (III.2)

Proof. To quantify the performance loss, we employ a conformal scoring function defined as:

$$p(x) := \frac{|V_\theta(0, x_i) - V_{\pi_\theta}(0, x_i)|}{C_{max}}, \forall x \in \mathcal{S}^*$$

where the score function measures the alignment between the induced optimal policy and the value function.

Next, we sample N_p states from the state space \mathcal{S}^* and compute conformal scores for all sampled states. For a user-defined error rate $\alpha_p \in [0, 1]$, let ψ denote the $\frac{(N_p+1)\alpha_p}{N_p}$ quantile of the conformal scores. According to [27], the following property holds:

$$\mathbb{P}_{x \in \mathcal{S}^*} \left(\frac{|V_\theta(0, x_i) - V_{\pi_\theta}(0, x_i)|}{C_{max}} \leq \psi \right) \sim \text{Beta}(N_p - l + 1, l),$$

where $l = \lfloor (N_p + 1)\alpha_p \rfloor$.

Define E_p as:

$$E_p := \mathbb{P}_{x \in \mathcal{S}^*} \left(\frac{|V_\theta(0, x_i) - V_{\pi_\theta}(0, x_i)|}{C_{max}} \leq \psi \right).$$

Here, E_p is a Beta-distributed random variable. Using properties of CDF, we assert that $E_p \geq 1 - \epsilon_p$ with confidence $1 - \beta_p$ if the following condition is satisfied:

$$I_{1-\epsilon_p}(N_p - l + 1, l) \leq \beta_p, \quad (25)$$

where $I_x(a, b)$ is the regularized incomplete Beta function. From [28](8.17.5), it can be shown that $I_x(n - k, k + 1) = \sum_{i=1}^k \binom{n}{i} x^i (1-x)^{n-i}$. Hence, Equation (25) can be equivalently stated as:

$$\sum_{i=1}^{l-1} \binom{N_p}{i} \epsilon_p^i (1 - \epsilon_p)^{N_p - i} \leq \beta_p \quad (26)$$

Thus, if Equation (26) holds, we can conclude with probability $1 - \beta_p$ that:

$$\mathbb{P}_{x \in \mathcal{S}^*} \left(\frac{|V_\theta(0, x_i) - V_{\pi_\theta}(0, x_i)|}{C_{max}} \leq \psi \right) \geq 1 - \epsilon_p.$$

□

APPENDIX B

ADDITIONAL DETAILS OF THE SYSTEMS IN THE EXPERIMENTS

In this section, we will provide more details about the systems we have used in the experiments section IV.

A. 2D Boat

The states, x of the 2D Boat system are $x = [x_1, x_2]^T$, where, x_1, x_2 are the x and y coordinates of the boat respectively. We define the step cost at each step, $l(t, x)$, as the distance from the goal, given by:

$$l(t, x) := \|x - (1.5, 0)^T\|$$

The cost function $C(t, x(t))$ is defined as:

$$C(t, x(t), \mathbf{u}) = \int_t^T l(t, x(t)) dt + \phi(x(T)) \quad (27)$$

where T is the time horizon (2s in our experiment), $l(t, x(t)) = \|x(t) - (1.5, 0)^T\|$ represents the running cost, and $\phi(x(T)) = \|x(T) - (1.5, 0)^T\|$ is the terminal cost. Minimizing this cost drives the boat toward the island.

Consequently, the (augmented) dynamics of the 2D Boat system are:

$$\begin{aligned} \dot{x}_1 &= u_1 + 2 - 0.5x_2^2 \\ \dot{x}_2 &= u_2 \\ \dot{z} &= -l(t, x) \end{aligned}$$

where u_1, u_2 represents the velocity control in x_1 and x_2 directions respectively, with $u_1^2 + u_2^2 \leq 1$ and $2 - 0.5x_2^2$ specifies the current drift along the x_1 -axis.

The safety constraints are formulated as:

$$g(x) := \max(0.4 - \|x - (-0.5, 0.5)^T\|, 0.5 - \|x - (-1.0, -1.2)^T\|) \quad (28)$$

where $g(x) > 0$ indicates that the boat is inside a boulder, thereby ensuring that the super-level set of $g(x)$ defines the failure region.

1) *Ground Truth Comparison:* We compute the Ground Truth value function using the Level-Set Toolbox [17] and use it as a benchmark in our comparative analysis. To facilitate demonstration, unsafe states are assigned a high value of 20 instead of ∞ . The value function in this problem ranges from 0 to 14.76.

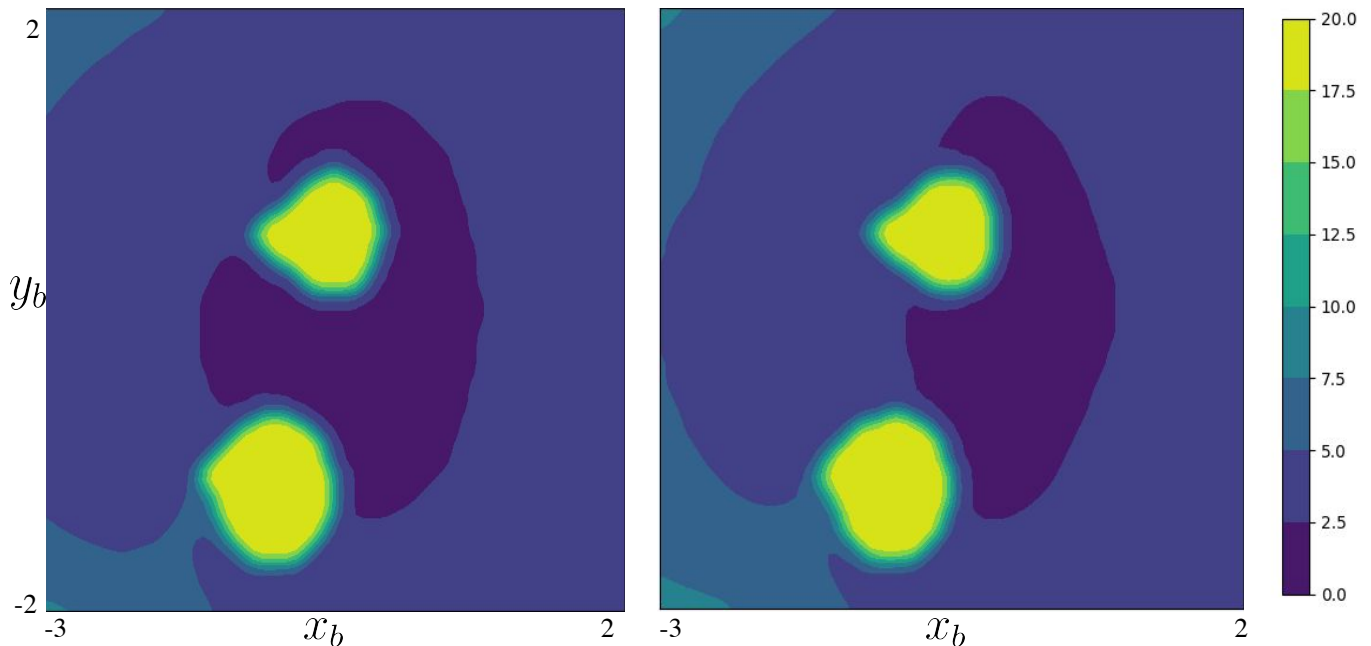


Fig. 7. Heatmap of the value function for the ground truth (left) and our method (right). The yellow region represents the unsafe area. Our method successfully captures most of the safe set, indicating that it is not overly conservative while completely recovering the unsafe regions.

As illustrated in Figure 7, the value function obtained using our method closely approximates the ground truth value function. Notably, the unsafe region (highlighted in yellow) remains identical in both cases, confirming the safety of the learned value function. Furthermore, the mean squared error (MSE) between the two value functions is 0.36, which is relatively low given the broad range of possible values.

It is also worth mentioning that computing a high-fidelity ground truth value function on a $210 \times 210 \times 210$ grid using the Level Set Toolbox requires approximately 390 minutes [29]. In contrast, our proposed approach learns the value function in 122 minutes, achieving a substantial speedup. This demonstrates that even for systems with a relatively low-dimensional state space, our method efficiently recovers an accurate value function significantly faster than grid-based solvers.

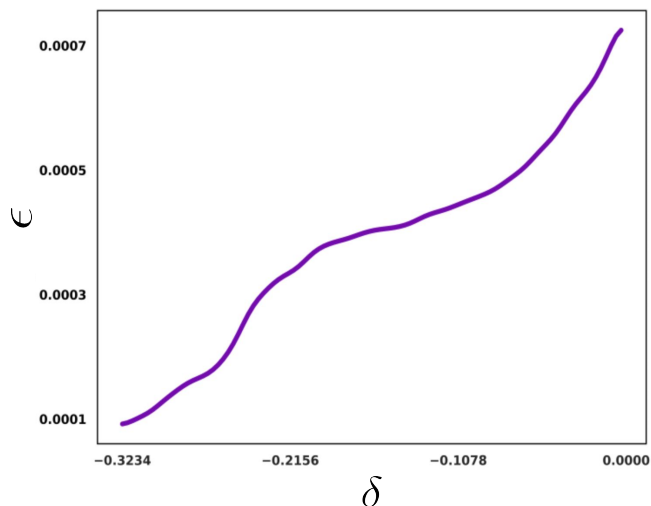


Fig. 8. δ versus ϵ for the learned auxiliary value function, $\hat{V}(t, \hat{x})$ after safety verification. It can be observed that δ varies with different safety violation levels, ϵ . Notably, δ approaches zero for sufficiently small ϵ , indicating that the learned value function exhibits very few safety violations.

2) *Calculation of Safety Levels:* Figure 8 illustrate the δ vs ϵ plot obtained after the safety verification algorithm proposed in Theorem III.1. We can observe that the δ level approaches 0 as the ϵ values approach the chosen safety level of 0.001. Hence,

we say that the sub-level set of the auxiliary value function, $\hat{V}(t, \hat{x})$ is safe with a probability of $1 - 0.001 = 0.999$.

B. Pursuer vehicle tracking an evader

The state, x of a ground vehicle (pursuer) tracking a moving evader is $x = [x_p, y_p, v, \Theta, x_e, y_e, v_{xe}, v_{ye}]^T$, where, x_e, y_e, v, Θ are position, linear velocity and orientation of the pursuer respectively, x_e, y_e, v_{xe}, v_{ye} are the position and the linear velocities of the evader respectively. We define the step cost at each step, $l(t, x)$, as the distance from the goal, given by:

$$l(t, x) := \|(x_p(t), y_p(t))^T - (x_e(t), y_e(t))^T\|$$

and the terminal cost is $\phi(x(T)) = \|(x_p(T), y_p(T))^T - (x_e(T), y_e(T))^T\|$. The cost function $C(t, x(t))$ is defined as:

$$C(t, x(t), \mathbf{u}) = \int_t^T l(t, x(t)) dt + \phi(x(T)) \quad (29)$$

where T is the time horizon (1s in this experiment). Minimizing this cost aims to drive the pursuer toward the evader. Consequently, the (augmented) dynamics of the system is as follows:

$$\begin{aligned} \dot{x}_p &= v \cos(\Theta) \\ \dot{y}_p &= v \sin(\Theta) \\ \dot{v} &= u_1 \\ \dot{\Theta} &= u_2 \\ \dot{x}_e &= v_{xe} \\ \dot{y}_e &= v_{ye} \\ \dot{v}_{xe} &= 0 \\ \dot{v}_{ye} &= 0 \\ \dot{z} &= -l(t, x) \end{aligned}$$

where u_1 represents the linear acceleration control and u_2 represents angular velocity control.

The safety constraints are defined as:

$$g(x) := \max(0.2 - \|x - (0.5, 0.5)^T\|, 0.2 - \|x - (-0.5, 0.5)^T\|, 0.2 - \|x - (-0.5, -0.5)^T\|, 0.2 - \|x - (0.5, -0.5)^T\|, 0.2 - \|x - (0.0, 0.0)^T\|,)$$

which represents 5 obstacles of radius 0.2 units each.

C. Multi-Agent Navigation

A multi-agent setting with 5 agents. The state of each agent i is represented by $x_i = [x_{a_i}, y_{a_i}, x_{g_i}, y_{g_i}]$, tries to reach its goal while avoiding collisions with others. (x_{a_i}, y_{a_i}) denote the position of the i th agent, while (x_{g_i}, y_{g_i}) represent the goal locations for that agent. We define the step cost at each step, $l(t, x(t))$, as the mean distance of each agent from its respective goal, given by:

$$l(t, x(t)) := \frac{\sum_{i=1}^5 \|(x_{a_i}(t), y_{a_i}(t))^T - (x_{g_i}(t), y_{g_i}(t))^T\|}{5}$$

The cost function $C(t, x(t), \mathbf{u})$ is defined as:

$$C(t, x(t), \mathbf{u}) := \int_t^T l(t, x(t)) dt + \phi(x(T)) \quad (30)$$

where T is the time horizon (2s in this experiment). Minimizing this cost aims to drive each agent towards its goal. Consequently, the (augmented) dynamics of the system is as follows:

$$\begin{aligned} \dot{x}_{a_i} &= u_{1i}, \forall i \in \{1, 2, 3, 4, 5\} \\ \dot{y}_{a_i} &= u_{2i}, \forall i \in \{1, 2, 3, 4, 5\} \\ \dot{x}_{g_i} &= 0, \forall i \in \{1, 2, 3, 4, 5\} \\ \dot{y}_{g_i} &= 0, \forall i \in \{1, 2, 3, 4, 5\} \\ \dot{z} &= -l(t, x) \end{aligned}$$

where u_{1i}, u_{2i} represents the linear velocity control of each agent i . The safety constraints are defined as:

$$g(x(t)) := \max_{i,j=\{1,\dots,5\}, i \neq j} (R - \|(x_{a_i}, y_{a_i})^T - (x_{a_j}, y_{a_j})^T\|) \quad (31)$$

APPENDIX C
IMPLEMENTATION DETAILS OF THE ALGORITHMS

This section provides an in-depth overview of our algorithm and baseline implementations, including hyperparameter configurations and the cost/reward functions used in the baselines across all experiments.

A. Experimental Hardware

All experiments were conducted on a system equipped with an 11th Gen Intel Core i9-11900K @ 3.50GHz \times 16 CPU, 128GB RAM, and an NVIDIA GeForce RTX 4090 GPU for training.

B. Hyperparameters for the Proposed Algorithm

We maintained training settings across all experiments, as detailed below:

Hyperparameter	Value
Network Architecture	Multi-Layer Perceptron (MLP)
Number of Hidden Layers	3
Activation Function	Sine function
Hidden Layer Size	256 neurons per layer
Optimizer	Adam optimizer
Learning Rate	2×10^{-5}
Boat Navigation	
Number of Training Points	65000
Number of Pre Training Epochs	50K
No. of Training Epochs	200K
Pursuer Vehicle Tracking Evader	
Number of Training Points	65000
Number of Pre Training Epochs	60K
No. of Training Epochs	300K
Multi Agent Navigation	
Number of Training Points	65000
Number of Pre Training Epochs	60K
No. of Training Epochs	400K

TABLE I
HYPERPARAMETERS FOR THE PROPOSED ALGORITHM

C. MPPI based baselines

For all the experiments we consider the MPPI cost term as follows:

$$C_{MPPI} = C(t, x(t), \mathbf{u}) + \lambda \max(g(x), 0) \quad (32)$$

where, λ is the trade-off parameter, $C(t, x(t), \mathbf{u})$, $g(x)$ are the cost functions and safety functions as defined in Appendix B. Following is the list of hyperparameters we have used for MPPI experiments in all the cases:

Hyperparameter	Value
Trade-off parameter (λ)	100
Planning Horizon	20
Softmax Lambda	200
No. of Rollouts	8000

TABLE II
HYPERPARAMETERS FOR MPPI BASELINES

D. C-SAC hyperparameters

For all the experiments, we consider the reward term as follows:

$$R_{CSAC} = -C(t, x(t), \mathbf{u}) - \mathbb{I}_{g(x) > 0} \times (100) + \mathbb{I}_{l(t, x(t)) < 0.1} \times (100) \quad (33)$$

where, $C(t, x(t), \mathbf{u})$, $g(x)$ are the cost functions and safety functions as defined in Appendix B. Following is the list of hyperparameters we have used for SAC experiments in all the cases:

E. Computation time Comparison

Figure 9 presents a comparative analysis of the offline and online computation times for our method against the baselines. It can be observed that the proposed approach exhibits better scalability with increasing dimensionality compared to C-SAC, as our method demonstrates a steady growth in training time, whereas C-SAC experiences a sharp increase in offline computation time as the dimensionality rises. Additionally, the online computation time for both our method and C-SAC remains significantly lower than that of online algorithms such as MPPI and MPPI-SF. This highlights the practicality of our method for real-time applications, provided that the offline value function has been precomputed.

Parameter	Value
Policy Architecture	Multi-Layer Perceptron (MLP)
learning rate	3×10^{-4}
buffer size	1,000,000
learning starts	10,000
batch size	256
Target network update rate (τ)	0.005
Discount factor (γ)	0.99
Boat Navigation	
Number of Training Steps	1,000,000
Pursuer Vehicle Tracking Evader	
Number of Training Steps	2,500,000
Multi Agent Navigation	
Number of Training Steps	1,000,000

TABLE III
GENERAL HYPERPARAMETERS OF SAC IN OUR EXPERIMENTS

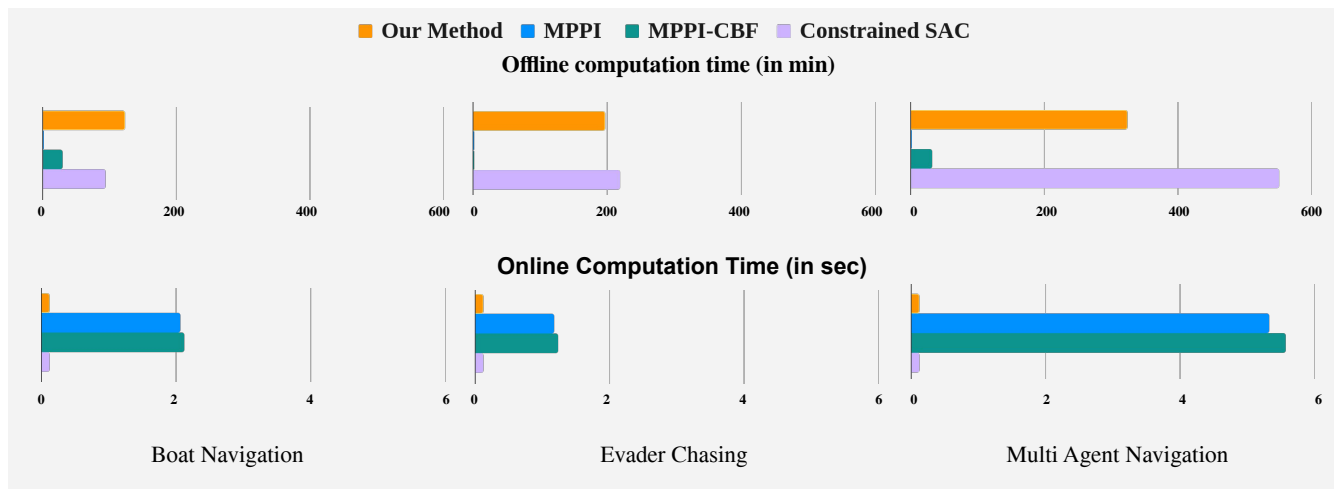


Fig. 9. This figure presents a comparative analysis of all methods based on online and offline computation time evaluated on the same computing machine. The top plot illustrates the **offline computation time** for our method and the baselines. Since our method and C-SAC involve training value functions, they incur higher offline computation costs, whereas MPPI-based methods require no offline training. The bottom plot depicts the **online computation time**, demonstrating that our method and C-SAC have minimal online computation requirements, whereas MPPI-based methods exhibit significantly higher online computational costs.

F. Comparison of Multi-Agent Navigation with baselines

Figures 10, 11, and 12 illustrate the trajectories obtained by the baseline methods for the Multi-Agent Navigation problem. It can be observed that the trajectories obtained by MPPI and MPPI-SF are highly conservative, implying that these methods prioritize safety to mitigate potential conflicts among agents. In contrast, the policy derived from C-SAC fails to maintain safety, resulting in agent collisions. This indicates that as system complexity increases, the baseline methods tend to prioritize either safety or performance, leading to suboptimal behavior and safety violations. Conversely, the proposed approach effectively co-optimizes safety and performance, even in complex high-dimensional settings, achieving superior performance while ensuring safety.

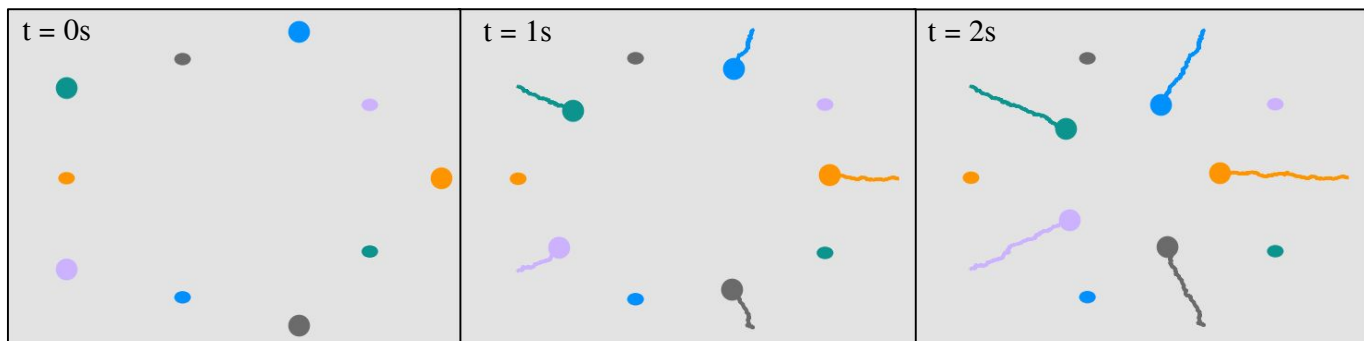


Fig. 10. Snapshots of multi-agent navigation trajectories at different time instances using MPPI. The trajectories indicate that the agents adopt a **highly conservative strategy** to prevent collisions. Consequently, this leads to a **reduction in performance**, as the agents **end up very far from their respective goals**.

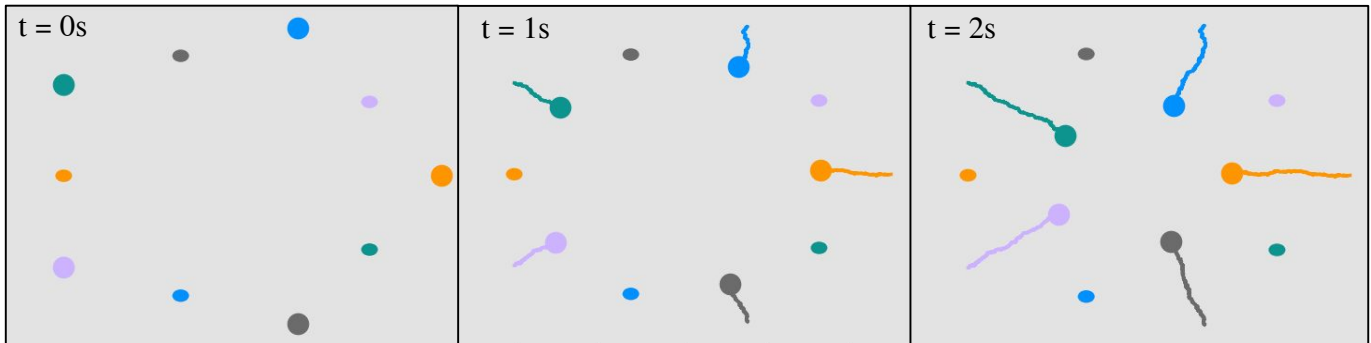


Fig. 11. Snapshots of multi-agent navigation trajectories at different time instances using **MPPI-NCBF**. The observed trajectories demonstrate **suboptimal behavior similar to that of the MPPI policy**. Consequently, this results in high-performance costs, indicating its **inability to effectively co-optimize safety and performance**.

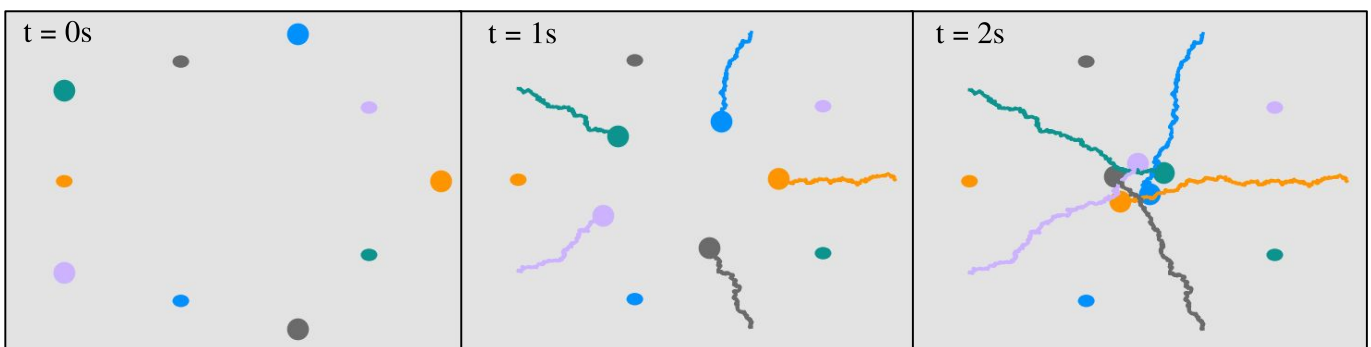


Fig. 12. Snapshots of multi-agent navigation trajectories at different time instances using **C-SAC**. The trajectories indicate that agents **demonstrate less conservative behavior compared to MPPI and MPPI-NCBF, but they lead to collisions**. These **safety violations are critical** and cannot be disregarded, further **highlighting the limitations of the baseline methods in simultaneously optimizing safety and performance**.